DOI 10.1007/s10527-020-09967-5
Biomedical Engineering, Vol. 54, No. 1, May, 2020, pp. 24-32. Translated from Meditsinskaya Tekhnika, Vol. 54, No. 1, Jan.-Feb., 2020, pp. 17-22.
Original article submitted November 14, 2019.

Determination of the Energy Efficiency of the Epicardium Using Magnetic Resonance Imaging with Contrast Enhancement in Patients with Cardiovascular Pathology

O. L. Bockeria[1], K. G. Potlovsky[2], V. N. Makarenko[1], T. G. Le[1]*, V. A. Shvartz[1], A. S. Satyukova[1], and M. B. Biniashvili[1]

Non-invasive MRI examination of the left ventricular free wall in cardiovascular patients can provide diagnostic data for determining the required energy efficiency and the implantation site of a power source converting the mechanical oscillations of the cardiac wall into electrical energy for powering an epicardial pacemaker.

Introduction

Currently, miniature devices for collecting non-electrical energy and converting it into electrical energy are being actively developed. Such converters are used to supply various autonomous low-power devices. In the field of biomedical engineering, this opens up new possibilities for developing power sources for medical implantable devices. The use of such converters makes it possible to increase the service life of the implantable devices and save patients from repeated surgical replacement of depleted galvanic batteries, which are the main power source of modern implantable devices. They also open the prospect for further miniaturization of implantable devices, such as pacemakers, defibrillators, or biosignal recorders [1-3].

A significant increase in the longevity of power sources for implantable devices was achieved primarily by increasing the capacity of the galvanic batteries. This was done by replacing mercury–zinc batteries with lithium–iodine-polyvinylpyridine batteries [4]. However, if a battery is the only power source for a device, there remains a high probability of a sudden failure due to battery malfunction (for example, because of a hidden defect). Thus, building an alternative backup power source into the implantable device can increase its reliability. In this regard, the conversion of heart contractions into electrical energy seems to be the best option. Regardless of the physical activity, heart contractions are regular. The heart muscle is able to go through more than 2.5 billion cardiac cycles over 70 years, with an average heart rate of 70 beats per minute. This makes it a reliable power source for modern pacemakers with a power consumption of up to 8 mW [5].

When choosing where on the epicardium to implant an electromechanical converter, it is necessary to take into account the following requirements:

1) vessels should be absent at the implantation site;

2) the epicardial velocity should be sufficient for the converter to produce electric power equal to or greater than that consumed by the implant.

The first requirement is mandatory to prevent injury. The second requirement follows from the principle of functioning of the electromechanical converter and is, in fact, the definition of energy efficiency of the epicardium.

In general terms, energy efficiency can be defined as the sum of the kinetic energies of translational and circular motion in the epicardial region that is in contact with the converter.

The possibilities of magnetic resonance imaging (MRI) with contrast enhancement for non-invasive diagnostic examination of the heart are numerous. In this work, MRI with contrast enhancement has been used as a

[1] Bakoulev National Medical Research Center for Cardiovascular Surgery, Ministry of Health of Russian Federation, Moscow, Russia; E-mail: tgle@bakulev.ru
[2] OOO Tekhnoportnoi, Moscow, Russia.
* To whom correspondence should be addressed.

basis for a technique for determining the best site for implantation of a wireless epicardial pacemaker with a MEMS-converter on the epicardium of a cardiovascular patient.

Patients with cardiovascular diseases were divided into 6 groups:

1) patients with cardiac arrhythmias and conduction disorders scheduled for Labyrinth-III B surgery;

2) patients with dilated cardiomyopathy;

3) patients with mitral valve diseases of various etiologies;

4) patients with congenital heart defects (atrial septal defect) over the age of 45 years;

5) patients with coronary heart disease with damaged right coronary artery;

6) patients with cardiac conduction disorders scheduled for pacemaker implantation.

These groups were selected because they exhibit the highest rate of conditions requiring electrotherapy: arrhythmias, conduction disturbances, and heart failure. Given the fact that almost all patients from these groups are scheduled for surgery with sternotomy and cardiopulmonary bypass, epicardial systems for electrotherapy of the heart are a priority for such patients.

Patients aged 45 to 65 years were selected for participation in the study to provide higher statistical comparability of the data obtained.

The patients selected for participation should also be without a history of allergic reactions. A contrast agent should be injected into their bloodstream, which can cause formidable complications in patients with a history of allergies.

Requirements for Equipment for Experimental Research

An MRI device from any manufacturer, with a magnetic field of 1.5 or 3 T, is required to obtain high-quality images. For bolus administration of a contrast agent, a system for a synchronized supply of contrast agent during the required phases of the cardiac cycle should be used.

Further post-processing analysis of images requires software for evaluating the displacement and speed of movement of different parts of the left ventricle at the epicardium level.

In this work, CVI-42 software was used to process MR images. The results of processing of each MR image were stored in a file containing data on radial, circular, and longitudinal deformations of the myocardium during the cardiac cycle.

CMR tissue tracking is a modern technology for evaluating the regional function of the left and right ventricles (myocardial deformation), including the circumference, longitudinal and radial deformations, as well as the deformation rate and time.

The use of electromagnetic converters in epicardial pacemakers makes it possible to use heart contractions as a source of power for pacemakers. The electromagnetic converter is designed so as to provide variation of the magnetic field penetrating the turns of the coil. A high-remanence permanent magnet is used as a source of the magnetic field. As the magnet rotates relative to a multi-turn conductive coil, an electromotive force (EMF) is induced in the coil in proportion to the rate of variation of the magnetic flux and the number of turns. Earlier, we proposed a mathematical model for calculating the energy efficiency of a specific area of the left ventricular free wall. The obtained MRI data is loaded into the tissue tracking module of the MRI data processing software. The results of tissue tracking are stored in an Excel file. It contains data on the radial, circular, and longitudinal deformations of the myocardium, pericardium, and epicardium per cardiac cycle for the selected cross section of a three-dimensional heart model. Since the amount of data is redundant, while the calculation requires only the data for the epicardium, a macro was compiled to extract these data from the lines marked as "epi" (i.e., containing values related to the epicardium). Then, the energy efficiency of a certain region of the left ventricular free wall is calculated taking into account the duration of systole and the power developed by the MEMS-converter sector. The intrinsic losses and the center of mass of the inertial sector are not taken into account.

Results

The results of processing of 40 MR images taken in patients from the 6 groups were analyzed. Potentially energy-efficient areas for the implantation of pacemakers were identified. These were areas with the velocity and displacement necessary for the electromechanical converter to produce the required electrical power.

The obtained data on the amplitude and velocity of displacement, the rotation, and the velocity of 16 segments underwent statistical analysis to determine the most energy-efficient areas of the left ventricular free wall at the epicardial level. These are the areas of choice for implanting an epicardial pacemaker with a MEMS-converter. The preferable implantation sites for each patient participating in the study are listed in Table 1.

The implantation sites are denoted in Table 1 as follows: 1 – basal segment of the anterior wall; 2 – basal segment of the anteroseptal wall; 3 – basal segment of the

TABLE 1. Preferable Implantation Sites for Each Patient

Protocol No. \ Segment	1	2	3	4	5	6	7	8	9	10	11	12	13	14	15	16
1	0	1	1	1	1	0	1	0	0	1	1	0	1	0	0	1
2	0	0	0	0	0	0	1	1	0	0	1	1	1	1	0	0
3	0	0	0	0	0	0	1	1	0	0	1	1	1	1	0	0
4	0	0	1	0	1	0	1	0	0	1	1	0	1	0	0	1
5	0	1	1	1	0	0	1	0	0	0	1	1	0	1	0	1
6	1	0	1	0	1	0	1	0	0	1	1	0	1	0	0	0
7	0	1	0	0	1	0	0	0	1	0	0	0	0	0	0	0
8	0	0	1	1	1	0	1	0	0	1	1	0	1	0	0	0
9	0	0	1	0	0	0	0	0	0	0	0	0	0	0	0	0
10	0	0	1	0	1	0	1	0	0	1	1	0	1	0	0	0
11	0	0	1	1	1	0	1	0	0	1	1	0	1	0	0	0
12	0	0	1	0	1	0	1	0	0	1	1	0	1	0	0	0
13	0	0	0	0	0	0	1	1	0	0	1	1	1	1	0	0
14	0	1	1	0	1	0	1	0	0	1	1	0	1	0	0	0
15	0	0	1	0	0	0	1	0	0	0	1	1	1	0	0	0
16	0	1	1	0	1	0	1	0	0	1	1	0	1	0	0	1
17	1	0	1	0	1	0	1	0	0	1	1	0	1	0	0	0
18	0	0	1	0	0	0	1	0	0	0	1	1	0	0	0	1
19	0	0	1	1	0	0	1	0	0	0	1	1	1	0	0	1
20	0	0	0	0	0	1	1	0	0	1	1	1	1	0	0	0
21	1	0	1	1	1	0	1	0	0	1	1	0	1	0	0	0
22	1	0	1	0	1	0	1	0	0	1	1	0	1	0	0	0
23	1	1	0	1	1	0	1	0	0	1	1	0	1	0	0	0
24	1	0	1	0	1	0	1	0	0	1	1	0	1	0	0	0
25	0	0	1	0	1	0	1	0	0	1	1	0	1	0	0	1
26	0	0	1	1	1	0	0	0	0	1	1	0	1	0	0	0
27	0	0	1	0	1	0	1	0	0	1	1	0	1	0	0	1
28	0	0	1	1	1	0	1	0	0	1	1	0	1	0	0	1
29	0	0	1	1	1	0	1	0	0	1	1	0	1	0	0	1
30	0	0	1	0	1	0	1	0	0	1	1	0	1	0	0	0
31	1	0	1	1	1	0	1	0	0	1	1	0	1	0	0	0
32	0	0	1	0	1	0	1	0	0	1	1	0	1	0	0	1
33	0	0	1	0	1	0	1	0	0	1	1	0	1	0	0	0
34	0	1	1	1	1	0	1	0	0	1	1	0	1	0	0	1
35	1	0	1	1	1	0	1	0	0	1	1	0	1	0	0	0
36	0	0	1	1	1	0	1	0	0	1	1	0	1	0	0	0
37	1	1	1	0	1	0	1	0	0	1	1	0	0	0	0	0
38	0	0	1	0	1	0	1	0	0	1	1	0	1	0	0	1
39	0	0	1	1	1	0	1	0	0	1	1	0	1	0	0	0
40	0	0	1	0	1	0	1	0	0	1	1	0	1	0	0	1

posteroseptal wall; 4 – basal segment of the posterior wall; 5 – basal segment of the posterolateral wall; 6 – basal segment of the anterolateral wall; 7 – middle segment of the anterior wall; 8 – middle segment of the anteroseptal wall; 9 – middle segment of the posteroseptal wall; 10 – middle segment of the posterior wall; 11 – middle segment of the posterolateral wall; 12 – middle segment of the anterolateral wall; 13 – apical segment of the anterior wall; 14 – apical septal segment; 15 – apical segment of the posterior wall; 16 – apical segment of the lateral wall.

Initially, the normality of the distribution of both quantitative and qualitative parameters was determined. Three tests for the normality of the distribution were used: Shapiro–Wilk (W), Kolmogorov–Smirnov (K-S), and Lilliefors (L), the Shapiro–Wilk test being the most stringent among the three. Figure 1 shows an example of a test for the normality of the distribution of some parameters under study.

It was found that the obtained data in most cases did not follow the normal distribution law. That is why further studies used techniques of parametric and, for the most part, nonparametric statistics.

The nonparametric Wilcoxon test and the parametric two-sample Student's t-test (for the normal distribution) were used to compare two dependent samples.

The nonparametric Friedman ANOVA test with the Bonferonni correction for the number of groups was used to compare several dependent samples.

The nonparametric Mann–Whitney test and the parametric two-sample Student's t-test (for the normal distribution) were used to compare two independent samples.

The nonparametric Kruskal–Wallis test with the Bonferonni correction for the number of groups was used to compare several independent samples.

Correlation analysis was performed using the nonparametric Spearman test and the parametric Pearson test. The correlation was considered high at $R > 0.7$; medium, at $R = 0.5$-0.7.

The data are presented as mean values and standard deviations $M \pm SD$ for a normal distribution or as the median and the interquartile range Me ($Q1$; $Q3$) for a non-normal distribution.

The reliability of the statistical estimates was taken as ≥95%. Microsoft Office Excel and Statsoft STATISTICA 10.0 were used for statistical processing.

Comparison between the groups (several independent groups) was carried out using the Kruskal–Wallis test. The obtained values of statistical significance are given in Table 2.

For segment 11 (middle segment of the posterolateral wall), there is a statistical difference between the groups 2 (patients with dilated cardiomyopathy) and 3 (mitral valve diseases of various etiologies) (Figs. 1 and 2).

Next, the frequencies were calculated to determine the most advantageous implantation sites for the groups of cardiovascular patients.

In the group of patients with cardiac arrhythmias and conduction disorders scheduled for Labyrinth III B surgery, the preferable implantation sites are the middle segments of the anterior and posterior walls of the left ventricle, as well as the apical segment of the anterior wall (Table 3).

In the group of patients with dilated cardiomyopathy, the preferable implantation sites are the basal segments of the anterior, lateral, and posterior walls of the left ventricle, as well as the middle segment of the anterior wall (Table 4).

In the group of patients with mitral valve diseases of various etiologies, the preferable implantation sites are the middle segments of the anterior, lateral, and posterior walls of the left ventricle, as well as the apical segment of the anterior wall (Table 5).

In the group of patients with congenital heart disease (atrial septal defect) over the age of 45 years (group 4), the preferable implantation sites are the middle segments of the anterior, lateral, and posterior walls of the left ventricle, as well as the apical segment of the anterior wall (Table 6).

In the group of patients with coronary heart disease with damaged right coronary artery (group 5), the preferable implantation sites are the middle segments of the anterior and lateral walls of the left ventricle, as well as the apical segment of the anterior wall (Table 7).

In the group of patients with impaired cardiac conduction scheduled for implantation, the preferable implantation sites are the basal segment of the lateral wall and the middle segments of the anterior and lateral walls of the left ventricle, as well as the apical segment of the anterior wall (Table 8).

The Tables 3-8 give the probabilities for the preferable implantation sites.

Statistical analysis of data on energy efficiency in cardiovascular patients makes it possible to compile clinical recommendations for the implantation of wireless epicardial pacemakers with a MEMS-converter. The results of these studies can also form the basis for practical recommendations for the use of miniature wireless epicardial single- and dual-chamber pacemakers with a MEMS-converter in patients with cardiovascular pathologies.

According to the data obtained, the preferable sites for implantation of a wireless epicardial pacemaker with a

TABLE 2. Statistical Difference between the Groups

Parameter	Value	Parameter	Value
Segment 1		*Segment 5*	
Radial displacement, mm, max	0.149	Radial displacement, mm, max	0.145
Circular displacement, deg, max	0.081	Circular displacement, deg, max	0.145
Maximum radial displacement time, ms	0.081	Maximum radial displacement time, ms	0.145
Maximum circular displacement time, ms	0.081	Maximum circular displacement time, ms	0.145
Maximum systolic speed of radial displacement, mm/s	0.081	Maximum systolic speed of radial displacement, mm/s	0.145
Maximum systolic speed of circular displacement, deg/s	0.081	Maximum systolic speed of circular displacement, deg/s	0.145
Maximum diastolic speed of radial displacement, mm/s	0.081	Maximum diastolic speed of radial displacement, mm/s	0.145
Maximum diastolic speed of circular displacement, deg/s	0.149	Maximum diastolic speed of circular displacement, deg/s	0.145
Segment 2		*Segment 6*	
Radial displacement, mm, max	0.081	Radial displacement, mm, max	0.206
Circular displacement, deg, max	0.085	Circular displacement, deg, max	0.270
Maximum radial displacement time, ms	0.259	Maximum radial displacement time, ms	0.057
Maximum circular displacement time, ms	0.081	Maximum circular displacement time, ms	0.344
Maximum systolic speed of radial displacement, mm/s	0.081	Maximum systolic speed of radial displacement, mm/s	0.159
Maximum systolic speed of circular displacement, deg/s	0.159	Maximum systolic speed of circular displacement, deg/s	0.087
Maximum diastolic speed of radial displacement, mm/s	0.159	Maximum diastolic speed of radial displacement, mm/s	0.093
Maximum diastolic speed of circular displacement, deg/s	0.845	Maximum diastolic speed of circular displacement, deg/s	0.719
Segment 3		*Segment 7*	
Radial displacement, mm, max	0.369	Radial displacement, mm, max	0.298
Circular displacement, deg, max	0.855	Circular displacement, deg, max	0.398
Maximum radial displacement time, ms	0.572	Maximum radial displacement time, ms	0.089
Maximum circular displacement time, ms	0.963	Maximum circular displacement time, ms	0.171
Maximum systolic speed of radial displacement, mm/s	0.365	Maximum systolic speed of radial displacement, mm/s	0.070
Maximum systolic speed of circular displacement, deg/s	0.853	Maximum systolic speed of circular displacement, deg/s	0.122
Maximum diastolic speed of radial displacement, mm/s	0.425	Maximum diastolic speed of radial displacement, mm/s	0.189
Maximum diastolic speed of circular displacement, deg/s	0.085	Maximum diastolic speed of circular displacement, deg/s	0.124
Segment 4		*Segment 8*	
Radial displacement, mm, max	0.657	Radial displacement, mm, max	0.206
Circular displacement, deg, max	0.571	Circular displacement, deg, max	0.190
Maximum radial displacement time, ms	0.340	Maximum radial displacement time, ms	0.927
Maximum circular displacement time, ms	0.732	Maximum circular displacement time, ms	0.148
Maximum systolic speed of radial displacement, mm/s	0.248	Maximum systolic speed of radial displacement, mm/s	0.184
Maximum systolic speed of circular displacement, deg/s	0.110	Maximum systolic speed of circular displacement, deg/s	0.295
Maximum diastolic speed of radial displacement, mm/s	0.192	Maximum diastolic speed of radial displacement, mm/s	0.190
Maximum diastolic speed of circular displacement, deg/s	0.502	Maximum diastolic speed of circular displacement, deg/s	0.279

TABLE 2 (Contd.)

Parameter	Value	Parameter	Value
Segment 9		*Segment 13*	
Radial displacement, mm, max	0.184	Radial displacement, mm, max	0.226
Circular displacement, deg, max	0.196	Circular displacement, deg, max	0.373
Maximum radial displacement time, ms	0.126	Maximum radial displacement time, ms	0.759
Maximum circular displacement time, ms	0.763	Maximum circular displacement time, ms	0.403
Maximum systolic speed of radial displacement, mm/s	0.270	Maximum systolic speed of radial displacement, mm/s	0.215
Maximum systolic speed of circular displacement, deg/s	0.671	Maximum systolic speed of circular displacement, deg/s	0.193
Maximum diastolic speed of radial displacement, mm/s	0.190	Maximum diastolic speed of radial displacement, mm/s	0.190
Maximum diastolic speed of circular displacement, deg/s	0.485	Maximum diastolic speed of circular displacement, deg/s	0.180
Segment 10		*Segment 14*	
Radial displacement, mm, max	0.099	Radial displacement, mm, max	0.721
Circular displacement, deg, max	0.394	Circular displacement, deg, max	0.215
Maximum radial displacement time, ms	0.646	Maximum radial displacement time, ms	0.219
Maximum circular displacement time, ms	0.631	Maximum circular displacement time, ms	0.575
Maximum systolic speed of radial displacement, mm/s	0.058	Maximum systolic speed of radial displacement, mm/s	0.120
Maximum systolic speed of circular displacement, deg/s	0.103	Maximum systolic speed of circular displacement, deg/s	0.769
Maximum diastolic speed of radial displacement, mm/s	0.103	Maximum diastolic speed of radial displacement, mm/s	0.296
Maximum diastolic speed of circular displacement, deg/s	0.103	Maximum diastolic speed of circular displacement, deg/s	0.180
Segment 11		*Segment 15*	
Radial displacement, mm, max	0.150	Radial displacement, mm, max	0.153
Circular displacement, deg, max	0.101	Circular displacement, deg, max	0.180
Maximum radial displacement time, ms	0.890	Maximum radial displacement time, ms	0.298
Maximum circular displacement time, ms	0.203	Maximum circular displacement time, ms	0.753
Maximum systolic speed of radial displacement, mm/s	0.260	Maximum systolic speed of radial displacement, mm/s	0.229
Maximum systolic speed of circular displacement, deg/s	**0.032**	Maximum systolic speed of circular displacement, deg/s	0.653
Maximum diastolic speed of radial displacement, mm/s	**0.032**	Maximum diastolic speed of radial displacement, mm/s	0.190
Maximum diastolic speed of circular displacement, deg/s	0.145	Maximum diastolic speed of circular displacement, deg/s	0.215
Segment 12		*Segment 16*	
Radial displacement, mm, max	0.142	Radial displacement, mm, max	0.289
Circular displacement, deg, max	0.154	Circular displacement, deg, max	0.212
Maximum radial displacement time, ms	0.216	Maximum radial displacement time, ms	0.220
Maximum circular displacement time, ms	0.685	Maximum circular displacement time, ms	0.190
Maximum systolic speed of radial displacement, mm/s	0.333	Maximum systolic speed of radial displacement, mm/s	0.475
Maximum systolic speed of circular displacement, deg/s	0.110	Maximum systolic speed of circular displacement, deg/s	0.354
Maximum diastolic speed of radial displacement, mm/s	0.154	Maximum diastolic speed of radial displacement, mm/s	0.190
Maximum diastolic speed of circular displacement, deg/s	0.154	Maximum diastolic speed of circular displacement, deg/s	0.221
		Age	0.116
		Sex	0.520

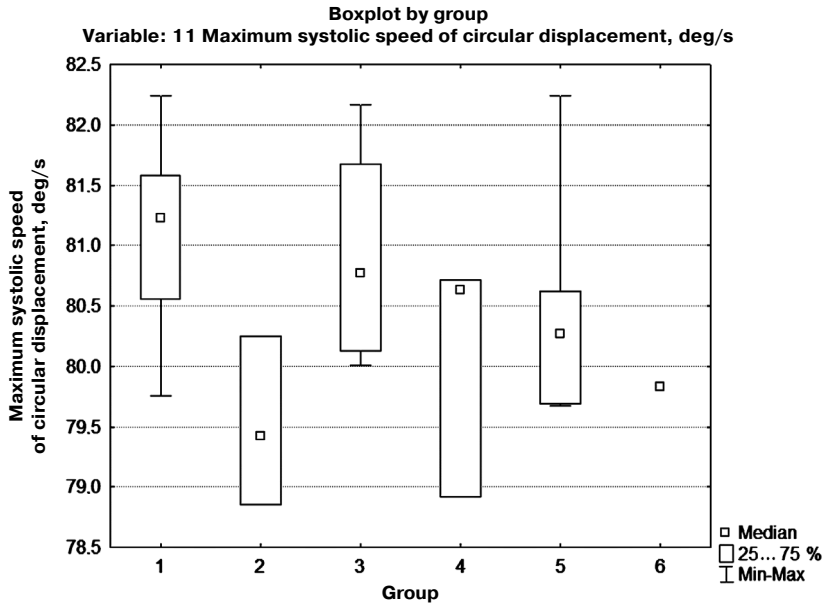

Fig. 1. Differences between the groups in the maximum systolic velocity of circular displacement of the middle segment of the posterolateral wall.

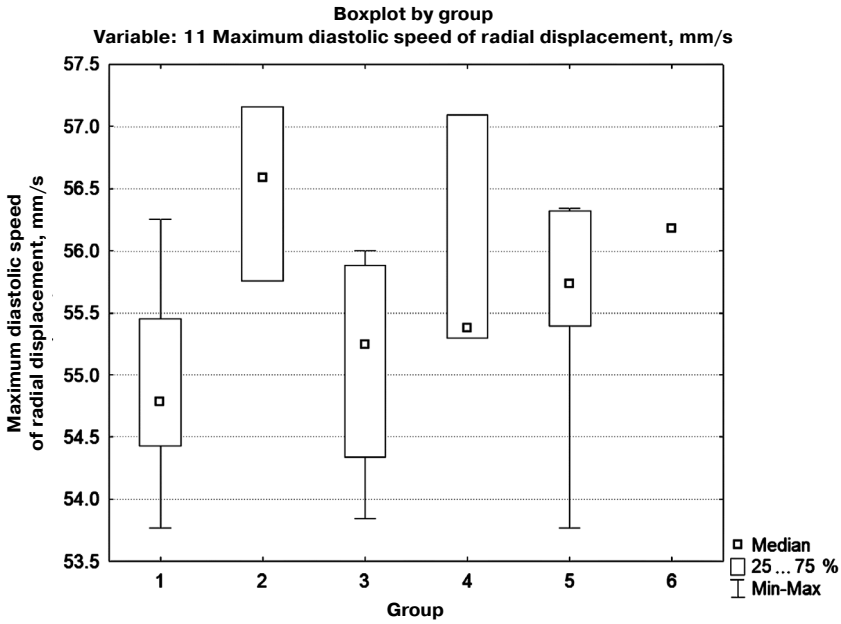

Fig. 2. Differences between the groups in the maximum diastolic velocity of radial displacement of the middle segment of the posterolateral wall.

MEMS-converter are the middle and apical segments of the anterior and anterolateral walls; the less preferable implantation sites are the posterior wall at the basal and middle levels.

Conclusions

The proposed method for calculating the energy efficiency of the epicardium of the left ventricular free wall

TABLE 3. Preferable Implantation Sites for Group 1

Segment	Frequency
1	27
2	13
3	87
4	40
5	80
6	0
7	93
8	7
9	0
10	80
11	100
12	20
13	87
14	7
15	0
16	47

TABLE 4. Preferable Implantation Sites for Group 2

Segment	Frequency
1	33
2	33
3	100
4	33
5	100
6	0
7	100
8	0
9	0
10	100
11	100
12	0
13	100
14	0
15	0
16	33

TABLE 5. Preferable Implantation Sites for Group 3

Segment	Frequency
1	0
2	45
3	91
4	45
5	81
6	0
7	81
8	0
9	9
10	73
11	81
12	9
13	72
14	9
15	0
16	36

TABLE 6. Preferable Implantation Sites for Group 4

Segment	Frequency
1	67
2	0
3	100
4	67
5	100
6	0
7	100
8	0
9	0
10	100
11	100
12	0
13	100
14	0
15	0
16	33

TABLE 7. Preferable Implantation Sites for Group 5

Segment	Frequency
1	29
2	0
3	57
4	0
5	57
6	14
7	100
8	29
9	0
10	71
11	100
12	42
13	100
14	29
15	0
16	0

TABLE 8. Preferable Implantation Sites for Group 6

Segment	Frequency
1	0
2	0
3	100
4	100
5	0
6	0
7	100
8	0
9	0
10	0
11	100
12	100
13	100
14	0
15	0
16	100

from the data obtained by MRI with contrast enhancement makes it possible to determine the best implantation sites for a wireless pacemaker with a MEMS-converter. Statistical analysis of data on energy efficiency in cardiovascular patients makes it possible to compile clinical recommendations for the implantation of wireless epicardial pacemakers with a MEMS-converter. It is planned to continue the research in this direction. These studies will also form the basis for practical recommendations for the use of miniature wireless epicardial single- and dual-chamber pacemakers with a MEMS-converter in patients with cardiovascular diseases.

This study was supported by the Russian Ministry of Education and Science grant No. 14.607.21.0192 "Creation of a Lineup of Miniature Wireless Epicardial Pacemakers with MEMS-converters for the Treatment of Bradycardia and Cardiac Failure" (unique contract identifier RFMEFI60717X0192).

REFERENCES

1. Bockeria, O. L., Potlovsky, K. G., Bazhin, M. A., Glushko, L. A., Satyukova, A. S., Le, T. G., and Shvartz, V. A., "Potential for use of heart contractions as a source of energy for implantable devices," Biomed. Eng., **52**, 412-415 (2019).
2. Pfeninger, A., Jonsson, M., Zurbuchen, A., Koch, V. M., and Vogel, R., "Energy harvesting from the cardiovascular system or how to get a little help from yourself," Ann. Biomed. Eng., **41**, No. 11, 2248-2263 (2013).
3. Zurbuchen, A., Pfeninger, A., Stahel, A., Stoeck, C. T., Vandenberghe, S., Koch, V. M., and Vogel, R., "Energy harvesting from the beating heart by a mass imbalance oscillation generator," Ann. Biomed. Eng., **41**, No. 1, 131-141 (2013).
4. Untereker, D. F., Schmidt, C. L., Prabhakar, G. J., Tamirisa, A., Hossick-Schott, J., and Viste, M., "Power sources and capacitors for pacemakers and implantable cardioverter-defibrillators," in: Clinical Cardiac Pacing, Defibrillation and Resynchronization Therapy (2017), pp. 251-269.
5. Wong, L.S., Hossain, S., Ta, A., Edvinsson, J., Rivas, D. H., and Naas, H., "A very low-power CMOS mixed-signal IC for implantable pacemaker applications," IEEE J. Solid-State Circuits, **39**, 2446-2456 (2004).